Semiconductor Physics, Quantum Electronics & Optoelectronics, 2011. V. 14, N 1. P. 21-30.

PACS 73.22-f, 78.67.Ch, 81.07.De

Hydrothermal synthesis and properties of titania nanotubes doped with Fe, Ni, Zn, Cd, Mn

M.R. Kulish[1] V.L. Struzhko[2], V.P. Bryksa[1], A.V. Murashko[2], V.G. Il'in[2]
[1]V. Lashkaryov Institute of Semiconductor Physics, NAS of Ukraine
41, prospect Nauky, 03028 Kyiv, Ukraine
[2]L. Pisarzhevskiy Institute of Physical Chemistry, NAS of Ukraine
31, prospect Nauky, 03028 Kyiv, Ukraine
Corresponding author e-mail: n_kulish@yahoo.com

Abstract. Fe/TiO_2, Mn/TiO_2, Zn/TiO_2, Cd/TiO_2, Ni/TiO_2 titania nanotubes were synthesized by the method of direct hydrothermal synthesis. Their properties have been investigated using X-ray phase analysis and X-ray fluorescent analysis, high-resolution transmission electron microscopy, luminescent spectroscopy and Raman scattering. It has been ascertained that the Fe/TiO_2, Mn/TiO_2, Zn/TiO_2, TiO_2 titania nanotubes possess the structure of $Na_2Ti_2O_4(OH)_2$. The structure of Cd/TiO_2 titania, probably, is mixture of anatase and rutile phases. We have found that Fe, Mn, Zn, Cd, Ni does not form solid solution with TiO_2, and these metals are located in interlayer space. The mechanism of nanotube formation has been briefly discussed.

Keywords: titania, direct hydrothermal synthesis, nanotube.

Manuscript received 22.06.10; accepted for publication 02.12.10; published online 28.02.11.

1. Introduction

Simplicity and low cost of synthesis, high physical and chemical stability, nontoxicity of TiO_2 stimulated the search of ways to use this material in various industries. It is considered that TiO_2 must be used as photocatalyst [1, 2] or as electrodes in converters of solar energy to electric power [3, 4]. In both these cases, utilized is only a small part of sunlight energy, less than 8% [5]. It is related with a high bandgap value of TiO_2 modifications [6]. For instance, the direct energy gap of rutile TiO_2 modification is equal to 3.0±0.1 eV [6], brookite – 3.4±0.1 eV [6], anatase – 4.2 eV [7]. The indirect gap of anatase modification is equal to 3.2±0.1 eV [6].

In industrial applications, preference is usually shown for anatase modification, as it possesses higher photocatalytic activity as compared to rutile or brookite [8]. Any shift of optical response in the visible wavelength range due to doping TiO_2 with metals or non-metals, sensitization of TiO_2 with organic dyes or quantum dots possessing relatively narrow bandgaps (less than that of TiO_2) gives a positive effect for photocatalysis and the coefficient of solar energy conversion into the electric one. The deficiency of TiO_2 sensitization with dyes lies in dye degradation [7]. The deficiency of doping TiO_2 with quantum dots is in presence of percolation conductivity [7]. Doping metals and/or non-metals are free not only of these lacks but also open new possibilities to use TiO_2, for example, for creation of memory cells from TiO_2 doped with ferromagnetic atoms (Fe and Co) [9, 10]. From all the possible configurations (quantum dots, wires, bars, sheets, nanotubes) [11] in photocatalysts and solar cells, it is desirable to use structures with the most strongly developed surface. Being doped with metals and/or non-metals, nanotubes are these structures. There exist three variants to include atoms of metals or non-metals to TiO_2 nanotubes, which is accompanied with changing the bandgap of TiO_2. First, they can replace titanium (at cation doping) [12, 13] or oxygen (at anion doping) [12, 14]. When the concentration of impurity atoms is high (several percents), they can form the impurity band in the middle of forbidden band TiO_2 [13] or can form substitutional solid solutions with metal atoms instead of titanium ones [15, 16]. Second, doping atoms can occupy interstitial positions [14]. Third, atoms of metal and/or non-metal can take their place between the layers of TiO_2 (intercalation) [17, 18] or take place on the internal and external surfaces of nanotubes. From a great number of doping TiO_2 cations, we have used Fe, Ni, Zn, Cd, Mn cations because titania Fe/TiO_2[13], Mn/TiO_2 [13], Ni/TiO_2 [19], Zn/TiO_2 [20], Cd/TiO_2 [21]

have high photocatalytic activity. Comparison of properties inherent to these catalysts can be made only in case when these titanates are synthesized using the same method, as their crystalline structure, morphology, component composition depends on the synthesis conditions. From all the variety of physical (ion implantation, magnetron or thermal sputtering, laser ablation, etc.) and chemical (sol-gel method, hydrothermal, solvatethermal, direct oxidation, chemical and electrolytic deposition and so on) methods to synthesize doped TiO_2 [7, 12], we showed preference far the direct hydrothermal method because of its low cost, simplicity and reliability to control synthesis parameters (molar composition, temperature, time of synthesis, pressure).

The following methods were used to control parameters of the obtained samples. Morphology of the samples (length, thickness of walls of nanotubes and their architecture) was determined using a transmission X-ray microscope ПЭМ-125К (firm "SELMI", Sumy). Elemental composition of the samples was determined using the X-ray fluorescent microscope JEOL JSM 6490 LV (Japan). X-ray phase analysis of the samples was performed using the BRUKER-D8 X-ray diffractometer of the firm ADVANC with CuK_α radiation. Optical properties (luminescence, Raman scattering) were investigated at room temperature using microraman spectrometer (T64000 JobinYvons spectrometer) equipped with the argon-krypton (Spectra Physics Stability 2018_RMAr$^+$/Kr$^+$ laser) and helium-cadmium lasers. Excitation of the samples was carried out at the wavelengths 488.0 and 325 nm. Wavelengths of Raman scattering and luminescence were measured with uncertainties $0.1\,\mathrm{cm}^{-1}$ and 0.1 nm, accordingly. Specific surface areas of the samples were determined via low temperature nitrogen desorption.

2. Synthesis

We used the hydrothermal method to prepare TiO_2 nanotubes. Nanotubes were obtained by treating industrial TiO_2 of TC model (anatase, specific surface $S_{sp} = 12\ m^2/g$) in a 10 M NaOH aqueous solution at 150-160 °C for 6 days within an autoclave with Teflon liners. After that, the residue was separated by filtration, washed in 0.05 M nitric acid solution and distilled water to pH 7 of washing water. Then, the residue was dried first at room temperature for 20 hours, and further for 4 hours at 60 °C, with following calcination at 300-400 °C for 2 hours (with 1°/min temperature growth).

The nanotubes doped with metals were prepared as follows. 0.5 g of TiO_2 powder and calculated amount of $Fe(NO_3)_3{\cdot}9H_2O$, $NiCl_2{\cdot}6H_2O$, $Mn(CH_3COO)_2{\cdot}4H_2O$, $Zn(CH_3COO)_2{\cdot}2H_2O$, $3CdSO_4{\cdot}8H_2O$, accordingly, were dispersed in 30 ml 10 M water solution of NaOH. Reactionary mixture was mixed for 2 hours at room temperature to obtain homogeneous solution. The molar ratio of titanium:metal was equal to 20:1. Then, the reactionary mixture was transferred into a steel autoclave with teflon liners and added with 10 ml of distilled water. The hydrothermal and postsynthetic treatment were carried out in such a way as at the synthesis of titanium nanotubes that was not doped by metals.

3. Morphology and component composition

Analysis of transmission electron microscopic patterns (Fig. 1) allow to determine that initial TiO_2 (TC model) is powder, Ni/TiO_2 is mixture of plates of nanometer sizes and short (<20 nm) nanotubes with the opened ends. Other titanates also had a structure of nanotubes with the opened ends (Fig. 1). The shape of nanotubes is close to the cylindrical one along all their length. The value of internal and external diameters of nanotubes is shown in Table 1. The length of nanotubes is few tens to few hundred nanometers. The specific surface (S_{sp}) is also shown in Table 1. Chemical composition of the samples was determined using the X-ray fluorescence analysis. It is shown in Table 2. Elements with numbers larger than five in Periodic Table of elements were registered, but hydrogen content was not determined. The error in determination of component composition did not exceed 0.01%.

4. X-ray diffraction

X-ray investigations of the synthesized samples were performed using X-ray powder diffraction patterns. The basic features of these patterns are shown in Fig. 2. They are as follows:

1) The angular dependence of the intensity of diffraction peaks from TiO_2 TC model coincides with the standard diffraction pattern of polycrystalline anatase TiO_2 phase [22, 23] in which any preferred orientation is absent.
2) The angular dependence of the intensity of diffraction peaks from Cd/TiO_2 is indicative of mixture inherent to anatase and rutile modifications (Table 3).
3) The X-ray diffraction pattern of other hydrothermally modified TiO_2 structures coincide with a diffraction pattern from the $Na_2Ti_2O_4{\cdot}(OH)_2$ nanotubes (Table 4).
4) The difference in angular positions of reflections (Fig. 2, Tables 3 and 4) of TiO_2, Fe/TiO_2, Zn/TiO_2, Mn/TiO_2, Ni/TiO_2 nanotubes lies within errors of their determination.
5) The direct hydrothermal synthesis of titanate nanotubes in the presence of metal salts influences only on angular position of the reflection located in the vicinity of 10° (Fig. 2, Tables 3 and 4). This reflection characterizes the distance between adjacent layers in the wall of nanotubes. The angular position of this reflection allows estimating the distance *d* between layers in nanotubes (Table 1), according to the Bragg equation

$$d = \frac{\lambda}{2 \sin \Theta}, \quad (1)$$

where λ is the wavelength of X-rays (CuK_α radiation, $\lambda = 0.15406$ nm), Θ is the diffraction angle. The error of d determination is less than 0.02%.

6) We did not find any reflections inherent to lattices of metals (Na, Ni, Mn, Zn, Fe), their oxides and hydroxides (Table 2).
7) The intensity of reflections for hydrothermally modified TiO_2 structures is considerably less, while the half-width is higher than the analogical parameters of TiO_2 TC model. It is caused by insufficient crystallization of structures [28] and small amount of layers in the walls of nanotubes [29].

5. Raman scattering

We used the spectrometer Bruker FRA106 FT-Raman in geometry of quasi-inverse Raman scattering to study TiO_2 nanotubes at room temperature. As an excitation source for TiO_2, we used the argon laser operating at 514.5 nm. The laser power directed at the sample was equal to 20 mW. Raman spectra of doped and undoped TiO_2 nanotubes and initial TiO_2 (TC model) are shown in Fig. 3. The position of peaks inherent to the vibrational modes of TiO_2 (TC model) coincide with vibrational modes for TiO_2 anatase modification (Table 5) that were found using the group-theoretical analysis [30] and presented by Rigy [31].

The forms and spectral positions of vibrational modes for doped with metal and undoped TiO_2 nanotubes are close to each other (Fig. 3, Table 6). The

Table 1. Geometrical parameters of TiO_2 nanotubes undoped and doped with metal ions.

No.	Material	Interlayer distance, nm	External diameter, nm	Internal diameter, nm	Difference of diameters, nm	Number of layers	$S_{sp.}$, m^2/g
1	Ti^{4+}:Fe^{2+}	0.925	10.1	4.4	5.7	3.08	193
2	Ti^{4+}:Mn^{2+}	0.913	8.4	4.1	4.3	2.36	210
3	Ti^{4+}:Ni^{2+}	0.939					120
4	Ti^{4+}:Zn^{2+}	0.996					153
5	Ti^{4+}:Cd^{2+}	0.997	11.0	4.2	6.8	3.41	51
6	THT	0.996	9.0	4.15	4.85	2.43	205
7	TC	1.465					12

Table 2. Chemical composition of samples.

Synthesis conditions	TiO_2 %	Na_2O %	Al_2O %	SiO_2 %	P_2O_5 %	FeO %	MnO %	NiO %	CdO %	CaO %	ZnO %
TiO_2 (TC),	98.53		0.58		0.89						
Ti^{4+}:Fe^{2+} = 20:1 HTS 160 °C / 6 days, TA 300 °C	89.42	6.18	0.35	0.81		2.9					
Ti^{4+}:Mn^{2+} = 20:1 HTS 160 °C / 6 days, TA 300 °C	90.61	6.41	0.24	0.19			2.47				
Ti^{4+}:Ni^{2+} = 20:1 HTS 160 °C / 6 days, TA 300 °C	84.00	9.82	0.35	0.43				5.69			
Ti^{4+}:Zn^{2+} = 20:1 HTS 150 °C / 6 days, TA 300 °C	85.08	14.37	0.31	0.14		0.33					$< 10^{-2}$
Ti^{4+}:Cd^{2+} = 20:1 HTS 150 °C / 6 days, TA 300 °C	77.63	7.71	0.36						14.5		
TiO_2-THT HTS 150 °C /6 days, TA 300 °C	88.39	11.61									

HTS – hydrothermal synthesis, TA – thermal annealing.

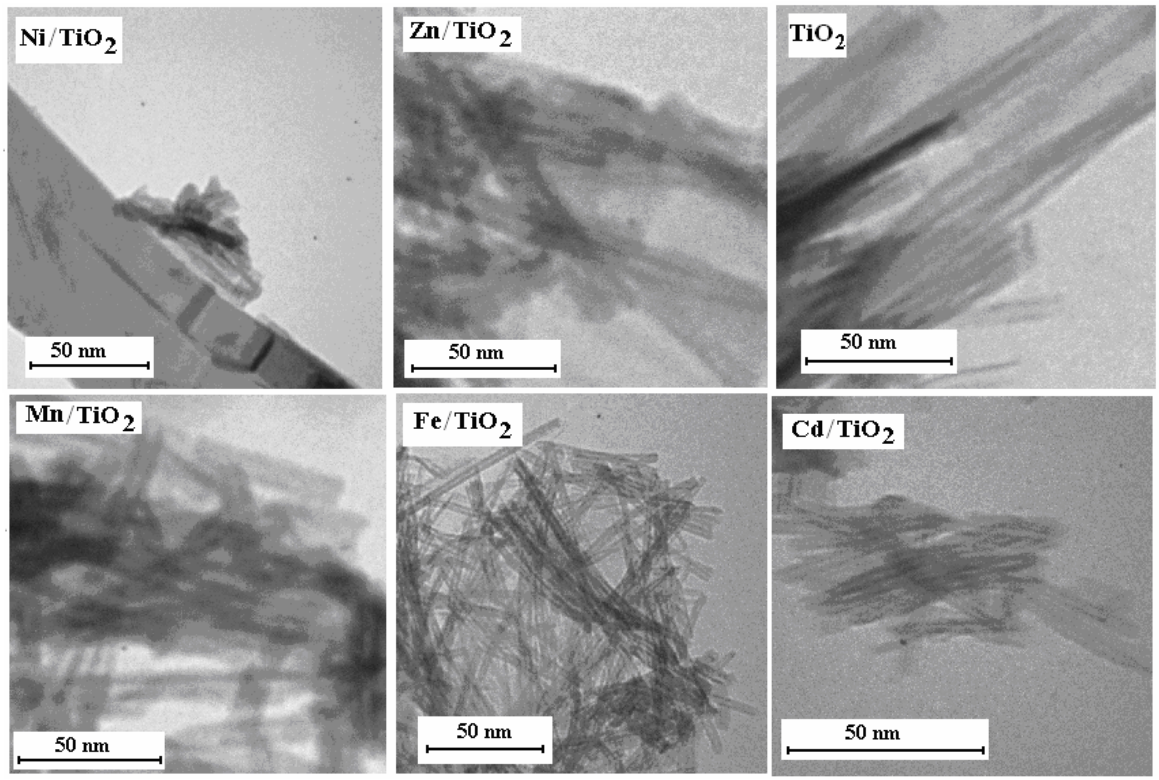

Fig. 1. Electron microscopy images of titanates.

vibrational modes of Cd/TiO_2 nanotubes belong to mixture modifications of rutile and anatase (Table 5). In Ni/TiO_2 nanotubes, one can observe only 4 vibrational modes peaking at 156.5, 277.8, 400, 600.8 cm^{-1}. The first three modes coincide with modes of brookite modification TiO_2, and the latter mode coincides with that of TiO_2 rutile modification.

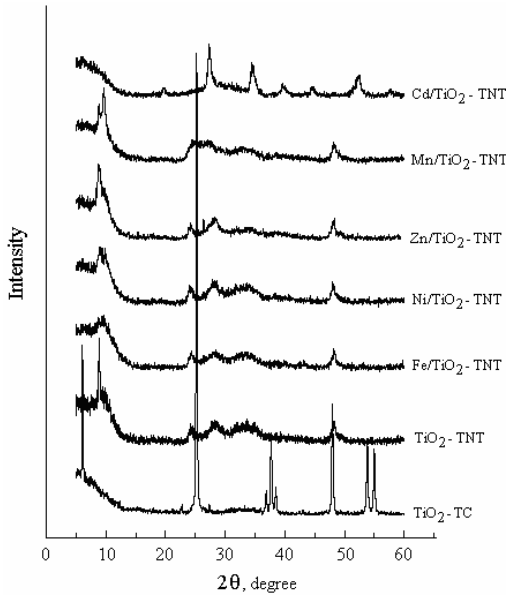

Fig. 2. X-ray diffraction patterns of initial TiO_2 (TC model) and titania nanotubes (TNT).

Hydrothermal treatment of initial TiO_2 (TC model) in the presence of metal salts in alkaline solution causes the following changes in spectra of Raman scattering (Fig. 3). 1) The width of peaks increases and their intensities decrease. 2) Raman scattering modes can shift by $\pm 20\,cm^{-1}$ relatively to peaks for initial TiO_2 (TC model). 3) The new vibrational modes appear (Tables 5 and 6). The first two factors are induced by the following factors: a confinement (by influence of sizes of nanotubes or grains) [32, 33]; temperature and number of calcinations, which determines the degree of

Table 3. Angular position of reflections of rutile and hydrothermally synthesized Cd/TiO_2 nanotubes.

Rutile (JCPDS) [24], 2θ, degree	Cd/TiO_2, 2θ, degree	Rutile [25], 2θ, degree	*hkl*
	6.16		
	19.8		
27.6	27.4	27.2	110
	34.5		
36.4	–	36.1	101
39.5	39.7	39.3	200
41.5	–	41.4	111
44.0	44.7	43.9	210
	52.4		
54.5	–	54.3	211
57.0	56.4	56.4	220

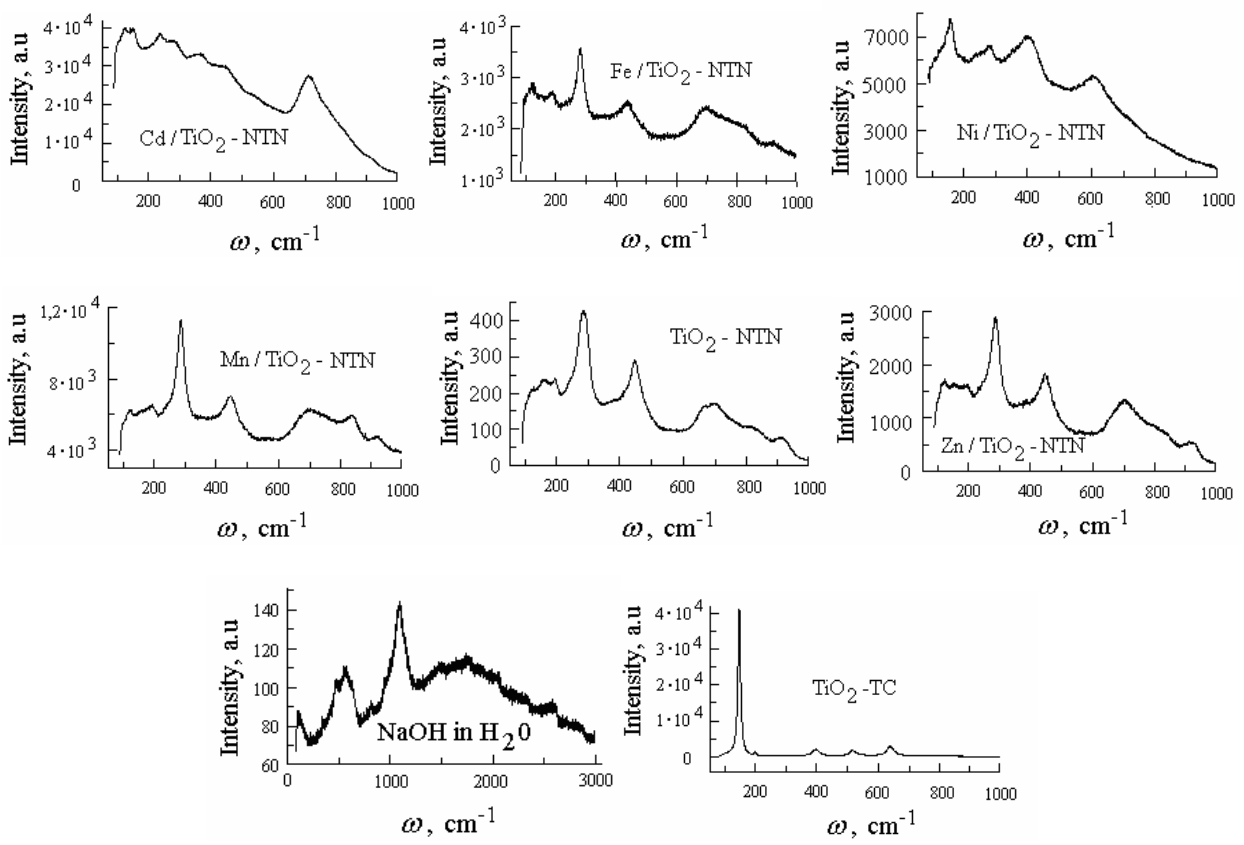

Fig. 3. Raman spectra of TiO_2 (TC model) and titania nanotubes (TNT).

crystallization of nanoparticles [32]; nonstoichiometry (more precisely to the oxygen deficit) [34, 35]. In particular, in Cd/TiO_2 the mode $\omega = 235\,cm^{-1}$ is the one of high-order vibration of $Ti-O-H$ bond [35, 36]; the mode $\omega = 126\,cm^{-1}$ arises from the $Na-O$ bond [35]. Appearance of the modes $\omega = (357-358)cm^{-1}$ and $\omega = 716\,cm^{-1}$ is possibly caused by the presence of some amount of $Cd(OH)_2$ or cadmium oxide that can appear in the process of hydrothermal synthesis of Cd/TiO_2.

In hydrothermally synthesized nanotubes (Table 6), the mode $\omega = (119-125)cm^{-1}$ characterizes vibration of the $Na-O$ bond [35], the modes $\omega = (151-158)cm^{-1}$ and $\omega = (189-192)cm^{-1}$ are analogical to vibrational E_g modes of TiO_2 in anatase modification [32], the modes $\omega = (283-286)cm^{-1}$ can characterize stretching vibrations of $Na-O-Ti$ bond [37], the mode $\omega = (442-447)cm^{-1}$ are E_g mode of rutile modification TiO_2 (Table 5), the mode $\omega = (910-926)cm^{-1}$ is characteristic for stretching vibration of $Ti=O$ or $Ti-O-Ti$ [33]. Nature of modes close to $\omega = (698-701)cm^{-1}$ needs additional investigations.

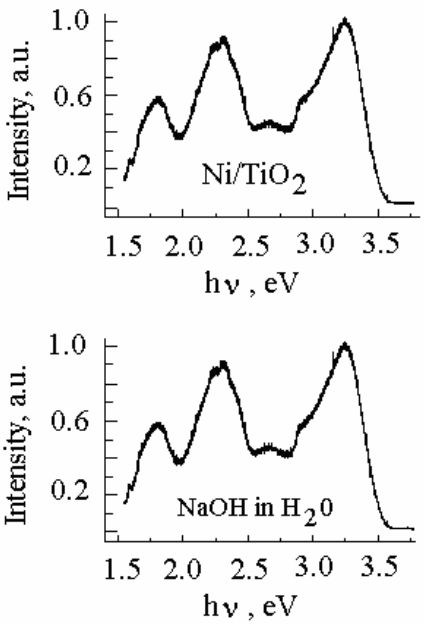

Fig. 4. Luminescence spectra of the titania nanotubes Ni/TiO_2 and NaOH aqueous solutions.

Table 4. X-ray diffraction of nanotubes made of $Na_2Ti_2O_4$, TiO_2, Mn/TiO_2, Zn/TiO_2, Fe/TiO_2 and Ni/TiO_2 titanates.

Ni/TiO_2, 2θ, degree	$Na_2Ti_2O_4·(OH)_2$ [26, 27], 2θ, degree	TiO_2, 2θ, degree	Mn/TiO_2, 2θ, degree	Zn/TiO_2, 2θ, degree	Fe/TiO_2, 2θ, degree	*hkl*
8.85	9.18	8.81	9.17	8.88	9.35	200*
25.00	24.30	24.24	24.22	24.16	24.45	110
27.95	28.14	28.37	28.15	28.22	28.22	600
32.96	34.24	32,83	33.40	32.80	33.15	301
38.65	3806	38.55		38.44	38.55	501
48.27	48.14	48.24	48.15	48.14	48.22	020
	61.76					002

*d_{200} is approximately equal to the distance between adjacent layers.

Table 5. Positions of band peaks for Raman scattering from initial TiO_2 (TC model) and Cd/TiO_2.

Anatase				Rutile			
GTA ω_m, cm^{-1} [30],	ω_m, cm^{-1} [31]	TiO_2-TC* ω_m, cm^{-1}	Mode	GTA ω_m, cm^{-1} [30]	ω_m, cm^{-1} [31]	Cd/TiO_2 ω_m, cm^{-1}	Mode
146.4	144	146.6	E_g			124	
	197	198.7	E_g	143	143	149	B_{1g}
396.9	399	396.8	B_{1g}		235	235	
518	519	516.3	A_{1g}/B_{1g}		357	358	
641.3	639	639.9	E_g	447	447		E_g
				612	612		A_{1g}
						716	
				826	826		B_{2g}

*Initial TiO_2, TC model.
GTA – group-theoretical analysis.

Table 6. Positions of band peaks for Raman scattering from titanates.

TiO_2, ω_m, cm^{-1}	Zn/TiO_2, ω_m, cm^{-1}	Mn/TiO_2, ω_m, cm^{-1}	Fe/TiO_2, ω_m, cm^{-1}
125	119	119	119
158	151		
192	192	190	189
283	286	284	283
447	449	444	442
698	701	699	700
910	920	920	926

6. Luminescence

Luminescence of titanates was researched at room temperature by using T64000 JobinYvons spectrometer. Spectra were excited with the radiation of a helium-neon laser (λ = 325 nm).

Presence of a large amount of surface defects gives rise to high speed of surface recombination. As a result, the TiO_2 luminescence photoresponse does not exceed 0.002 [38]. Luminescence of NaOH in aqueous solution with titanates prevents to research TiO_2 luminescence. At temperatures of calcination lower than 300 °C only physically adsorbed water remains. The intercalational OH-groups are observed both at temperatures lower than 300 °C and higher than 300 °C. In particular, the intercalational nickel atoms strongly interact with water that is present in the interlayer space. As a consequence, this water is incompletely eliminating from interlayer space at 300 °C temperature of calcination (Table 2). Thereof, these luminescence spectra of water and Ni/TiO_2 show complete (even in details) coincidence (Fig. 4). Luminescence of water prevails in other titanates, too (Fig. 5). Their spectra differ from each other only by different ratios for band intensities relatively to the most pronounced band (Fig. 5).

7. Discussion

TiO_2 belongs to the group of the layered crystals. Every layer consists of 3 monoatomic sheets (Fig. 6a). Interaction between atoms in a sheet is strong (Coulomb), and between layers it is weak (van-der-Waals) (Fig. 6b). Introduction of TiO_2 nanoparticles to water solution of NaOH or in mixture of water solution of NaOH and metal salt accompanied by adsorption of water molecules, OH-groups, sodium and metal atoms on surfaces of TiO_2 particles (Fig. 6c). The high orientational order of molecules comprising about 0.7 nm (approximately 2.5 monolayer of water) water layer is formed [39]. Between themselves, the molecules of water are related by hydrogen bonds. Oxygen of water and OH-groups forms a bond with surface atoms of TiO_2 [40, 41]. The metal ions form bonds like Ti – O – Na [35].

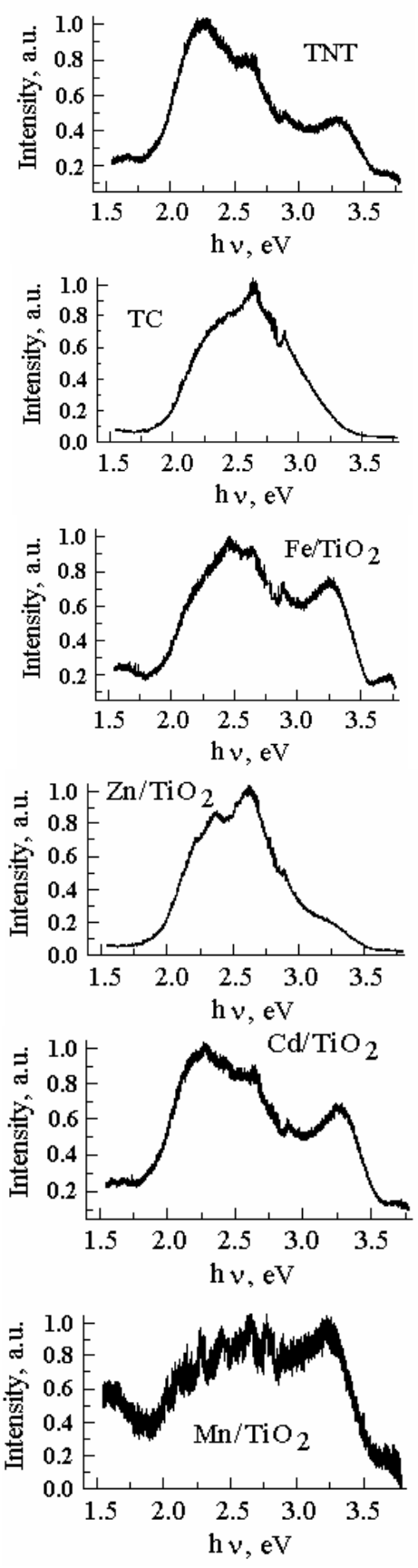

Fig. 5. Luminescence spectra of initial TiO_2 (TC model), undoped titania nanotubes (TNT) and doped titania nanotubes.

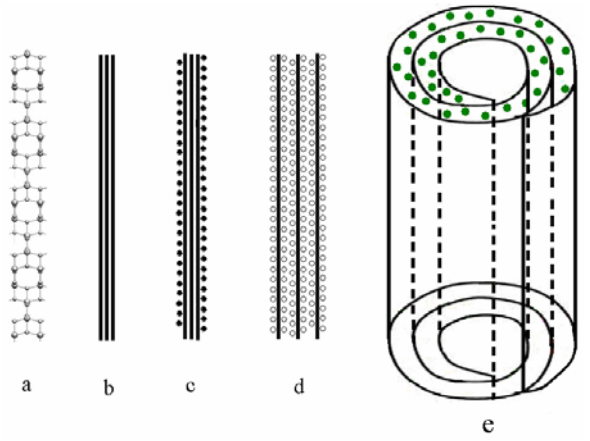

Fig. 6. Schematic drawing for formation of nanotubes. (a) is an anatase single layer (little spheres are the titanium atoms, large spheres are oxygen atoms); (b) is splitting of lamellar structures into nanosheets; (c) is the lamellar structure, on the external surface of which adsorption of molecules of water and NaOH (dark circles) take place; (d) is the lamellar structure, between sheets of which intercalated molecules of water and NaOH (light circles) are located; (e) is the image of a nanotube after hydrothermal synthesis (circles are molecules of water, atoms of hydrogen, OH-groups, metal oxides).

At hydrothermal treatment of TiO_2, there is diffusion of metal ions in the TiO_2 lattice and intercalation (Fig. 6d) of water molecules, OH-groups, metal ions (in case of modifying TiO_2 with metal ions) in interlayer spaces of TiO_2 between (100) planes [42]. Metal salts react with alkaline solution, forming hydroxides and oxides (Fe_2O_3, NiO, MnO, ZnO, CdO, $Cd(OH)_2$). These compounds can be adsorbed on the external and interlayer surfaces of TiO_2 particles and can serve as nanocrystal seeds [43].

As a result of large amount of intercalated metal ions and water molecules, the van-der-Waals interaction force decreases, which is accompanied with increase of the interlayer distance, and finally there takes place delamination of initial titania by plates in thickness of a few sheets [44]. The sizes of these plates can be increased due to dissolution of small titanate particle and finish building of larger nanoparticles by the mechanism of dissolution/recrystallization [42, 44]. When the value of surface tension will exceed the value of the energy for interlayer attraction, the monolayer of TiO_2 break away from (100) surface of the TiO_2 nanoparticle and scroll round the direction [010] in a nanotube [42-46], the axis of which is oriented along the direction [001] [42]. As a consequence, all the metal ions and water molecules that are adsorbed on nanoplate surface will be found in the interlayer space (Fig. 6e) [43, 47]. Since nanotubes are formed in all the course of hydrothermal synthesis [49], hydroxides and oxides of metals during all this time are deposited on the external and internal surfaces of nanotubes. Minimization of the total energy for a single layer of titania acid $H_2Ti_3O_7$ with respect to the curvature radius of nanotube gives the radius value close

to 4.3 nm [44, 48]. With growth of the number of layers, the total energy increases and even for the number of layers equal to 4 becomes positive [44, 48]. It means that in the presence of such amount of layers the process of scrolling is stopped. Probably, an analogical process was observed in the nanotubes that are synthesized by us, although the number of layers in them is less than four (Table 1).

Washing the filtered residue with nitric acid solution allows to neutralize alkali. Then, washing the residue with distilled water allows to delete reaction products of acid with alkali from the surface of nanotubes. It is important to remember that washing the residue with nitric acid solution could not eliminate oxides and hydroxides of metals from the interlayer space.

The nanotubes washed in nitric acid solution and distilled water are crumbly and unstable. For their stabilization, the procedure of calcination was executed. Calcination of residue is accompanied by desorption of intercalated water, which causes diminishing the interlayer distance in titanates as compared to TiO_2 TC model (Table 1). This result conforms to information of works [17, 26]. However, there is desorption of mainly physically adsorbable water at the chosen temperature of calcination (300 °C) [26]. Among all the investigated metals, nickel intercalated to the interlayer space most strongly interacts with intercalated water [47], as a consequence, the largest value of water remains in Ni/TiO_2. As a result, one can observe a complete coincidence of luminescence spectra inherent to Ni/TiO_2 and NaOH aqueous solutions (Fig. 4). In other titanates, luminescence of NaOH aqueous solution dominates. It is indicative of the presence of a larger amount of water in the interlayer space of these titanates.

X-ray phase analysis and optical researches did not find out any formation of solid solutions like $M_xTi_{1-x}O_2$ (M is a metal from the row: Na, Fe, Mn, Ni, Zn, Cd). A most probable, these metals or their oxides are selected as a separate phase on the external surfaces of nanotubes (see, for example [50, 51]). Absence of X-ray reflections from metals and oxides is, possibly, stipulated by finding these compounds in the amorphous state.

8. Conclusions

The analysis of electron-microscopic, X-ray, optical data and mechanism of titania nanotubes formation permits us to draw the following conclusions. The optimum conditions for formation of modified with metal ions titania nanotubes have been ascertained. It has been found that the structure of Fe/TiO_2, Mn/TiO_2, Zn/TiO_2, TiO_2 nanotubes is similar to $Na_2Ti_2O_4{\cdot}(OH)_2$ structure. The structure of Cd/TiO_2 titanate, probably, is a mixture of anatase and rutile modifications. The investigated metals do not form a solid solution of metal with TiO_2. These metals are adsorbed on external and internal surfaces of nanotubes. It is set that the specific surface of titania nanotubes (50-210 m^2/g) considerably exceeds that of initial TiO_2 (12 m^2/g).

Acknowledgement

We are grateful to firm Global partner of TOKYO BOEKI Ltd. for the possibility to determine element composition of samples by using the electron microscope JEOL JSM 6490 LV (Japan). This work was supported by the Ukrainian complex program for fundamental researches of the National Academy of Sciences in accord with the project "Nanostructural systems, nanomaterials and nanotechnologies".

References

1. J. Li, J. Xu, Wei-Lin Dai, and K. Fan, Dependence of Ag deposition methods on the photocatalytic activity and surface state of TiO_2 with twist-like helix structure // *J. Phys. Chem. C,* **113***,* No.19, p. 8343-8349 (2009).
2. C. Ratanatawanate, Y. Tao, and K.J. Balkus, Photocatalytic activity of PbS quantum dot/TiO_2 nanotube composites // *J. Phys. Chem. C,* **113**, No.24, p. 10755-10760 (2009).
3. X.D. Li, D.W. Zhang, Z. Sun, Y.W. Chen, S.M. Huang, Metal-free indoline-dye-sensitized TiO_2 nanotube solar cells // *Microelectronics J.*, **40**, No.1, p. 108-114 (2009).
4. M. Gratzel, Conversion of sunlight to electric power by nanocrystalline dye-sensitized solar cells // *J. Photochem. and Photobiol. A: Chemistry*, **164**, No.1, p. 3-14 (2004).
5. W. Hu, L. Li, G. Li, C. Tang and L. Sun, High-quality brookite TiO_2 flowers: synthesis, characterization, and dielectric performance // *Crystal Growth & Design*, **9**, No.8, p. 3676-3682 (2009).
6. G.K. Mor, O.K. Varghese, M. Paulose, K. Shankar, and C.A. Grimes, A review on highly ordered, vertically oriented TiO_2 nanotube arrays: Fabrication, material properties, and solar energy applications // *Solar Energy Materials and Solar Cells*, **90**, No.14, p. 2011-2075 (2006).
7. K. Shankar, J.I. Basham, N.K. Allam, O.K. Varghese, G.K. Mor, X. Feng, M. Paulose, J.A. Seabold, K.-S. Choi, and C.A. Grimes, Recent advances in the use of TiO_2 nanotube and nanowire arrays for oxidative photoelectrochemistry // *J. Phys. Chem. C*, **113**, No.16, p. 6329-6359 (2009).
8. T. Okato, T. Sakano, and M. Obaro, Suppression of photocatalitic efficiency in N-doped anatase films // *Phys. Rev.* **72**, No.11, p. 115124-115129 (2005).
9. J.M. Sullivan and S.C. Erwin, Theory of dopants and defects in Co-doped TiO_2 anatase // *arXiv:cond-mat/0211614v2.*

10. L.C.J. Pereira, M.R. Nunes, O.C. Monteiro, A.J. Silvestre, Magnetic properties of Co-doped TiO_2 anatase nanopowders // *arXiv.org > cond-mat > arXiv:0809.1256v2*.
11. D.J. Mowbray, J.I. Martinez, J.M.G. Lastra, K.S. Thygesen, and K.W. Jacobsen, Stability and electronic properties of TiO_2: nanostructures with and without B and N doping // *J. Phys. Chem.* **113**, No.28, p. 12301-12308 (2009).
12. X. Chen, S.S. Mao, Titanium dioxide nanomaterials: syntesis, properties, modifications, and applications // *Chem. Rev.* **107**, No.7, p. 2891-2959 (2007).
13. W. Choi, A. Termin, and M.R. Hoffmann, The role of metal ion depands in quantum-sized TiO_2: correlation between photoreactivity and charge carrier recombination dynamics // *J. Phys. Chem.* **98**, No.51, p. 13669-13679 (1994).
14. Y.-F. Tu, S.-Y. Huang, J.-P. Sang, and X.-W. Zou, Synthesis and photocatalytic properties of Sn-doped TiO_2: nanotube arrays // *J. Alloys and Compounds* **482**, No.1-2, p. 382-387 (2009).
15. W. Wunderlich, L. Miao, M. Tanemura, S. Tanemura, P. Jin, K. Kaneko, A. Terai, N. Nabatova-Gabin and R. Belkada, Ab-initio calculations of the optical band-gap of TiO_2 thin films // *Arxiv/condmat/0404222*.
16. Tian-hu Xu, Chen-lu Song, Yong Liu, Gao-rong Han, Band structures of TiO_2 doped with N, C and B // *J. Zhejiang Univ. SCIENCE B*, **7**, No.4, p. 299-303 (2006).
17. T. Sasaki, Y. Komatsy, Y. Fujiki, Protonated pentatitanate: preparation, characterizations, and cation intercalation // *Chem. Mater*., **4**, No.4, p. 894-899 (1992).
18. I.F. Mironyuk, V.V. Lobanov, B.K. Ostafiichuk, I.I. Grigorchak, R.V. Il'nitsky, Electron structure and properties of titanium dioxide intercalated with lithium // *Fizyka i khimiya tverd. tila*, **2**(3), p. 493-499 (2001), in Ukrainian.
19. Y. Oua, J. Lina, S. Fanga and D. Liao, MWNT–TiO_2:Ni composite catalyst: A new class of catalyst for photocatalytic H_2 evolution from water under visible light illumination // *Chem. Phys. Lett*., **429**, No. 1-3, p. 199-203 (2006).
20. T. Deguchi, K. Imai, H. Matsui, M. Iwasaki, H. Tada, S. Ito, Rapid electroplating of photocatalytically highly active TiO_2-Zn nanocomposite films on steel // *J. Mater. Sci.* **36**, No.19, p. 4723-4729 (2001).
21. L.A. Errico, G. Fabricius, M. Renterı, P. de la Presa, and M. Forker, Anisotropic relaxations introduced by Cd impurities in rutile TiO_2: First-principles calculations and experimental support // *Phys. Rev. Lett*., **89**, No.5, p. 055503-1 – 055503-4 (2002).
22. Joint Committee on Powder Diffraction Standards (JCPDS), Card No. 21-1272, Swurthmore, PA.
23. G. Liu, C. Sun, L. Cheng, Y. Jin, H. Lu, L. Wang, S.C. Smith, G.Q. Lu, H.-M. Cheng, Efficient promotion of anatase TiO_2 photocatalysis via bifunctional surface-terminating Ti-O-B-N structures // *J. Phys. Chem. C*, **113**, No.28, p. 12317-12324 (2009).
24. Joint Committee on Powder Diffraction Standards (JCPDS), Card No. 21-1276, Swurthmore, PA.
25. V. Samuel, R. Pasricha, V. Ravi, Synthesis of nanocrystalline rutile // *Ceramics Intern.* **31**, No.4, p. 555-557 (2005).
26. M. Zhang, Z. Jin, J. Zhang, X. Guo, J. Yang, W. Li, X. Wang, Z. Zhang, Effect of annealing temperature on morphology, structure and photocatalytic behavior of nanotubed $H_2Ti_2O_4{\cdot}(OH)_2$ // *J. Molecular Catalysis A: Chem.* **217**, No.1/2, p. 203-210 (2004).
27. S. Zhang, W. Li, Z. Jin, J. Yang, J. Zhang, Z. Du, Z. Zhang, Study on ESR and inter-related properties of vacuum-dehydrated nanotubed titanic acid // *J. Solid State Chem.* **177**, No.4/5, p. 1365-1371 (2004).
28. J. Yu, Y. Yu, B. Cheng, C. Trapalis, Effects of calcination temperature on the microstructures and photocatalytic activity of titanate nanotubes // *J. Molecular Catalysis A: Chem.* **249**, No.1/2, p. 135-142 (2006).
29. C.-C. Tsai, H. Teng, Regulation of the physical characteristics of titania. Nanotube aggregates synthesized from hydrothermal treatment // *Chem. Mater.* **16**, No.22, p. 4352-4358 (2004).
30. G.R. Hearne, J. Zhao, A.M. Dawe, V. Pischedda, M. Maaza, M.K. Nieuwoudt, P. Kibasomba, O. Nemraoui, and J.D. Comins, Effect of grain size on structural transitions in anatase TiO_2: A Raman spectroscopy study at high pressure // *Phys. Rev. B* **70**, 134102 (2004).
31. S.J. Rigby, A.H.R. Al-Obaidi, S.-K. Lee, D. McStay, P.K.J. Robertson, The application of Raman and anti-stokes Raman spectroscopy for in situ monitoring of structural changes in laser irradiated titanium dioxide materials // *Appl. Surf. Sci.* **252**, p. 7948-7952 (2006).
32. W. Ma, Z. Lu, M. Zhang, Investigation of structural transformations in nanophase titanium dioxide by Raman spectroscopy // *Appl. Phys. A* **66**, p. 621-627 (1998).
33. Y. Masuda, T. Ohji, K. Kato, Multineedle TiO_2 nanostructures, self-assembled surface coatings, and their novel properties // *Crystal Growth & Design*, **10**, No.2, p. 913-922 (2010).
34. C. Liu, S. Yang, Synthesis of angstrom-scale anatase titania atomic wires // ACS NANO **3**, No.4, p. 1025-1031 (2009).
35. L. Qian, Z.-L. Du, S.-Y. Yang, Z.-S. Jin, Raman study of titania nanotube by soft chemical process // *J. Molecular Structure* **749**, No. 1-3, p. 103-107 (2005).
36. S. Zhou, E. Čižmar, K. Potzger, M. Krause, G. Talut, M. Helm, J. Fassbender, S.A. Zvyagin, J. Wosnitza, H. Schmidt, Origin of magnetic

moments in defective TiO_2 single crystals // *Phys. Rev. B* **79**, 113201 (2009).
37. Y.V. Kolen'ko, K.A. Kovnir, A.I. Gavrilov, A.V. Garshev, J. Frantti, O.I. Lebedev, B.R. Churagulov, G. Van Tendeloo, M. Yoshimura, Hydrothermal synthesis and characterization of nanorods of various titanates and titanium dioxide // *J. Phys. Chem. B*, **110**, No.9, p. 4030-4038 (2006).
38. H.N. Ghosh, S. Adhikari, Trap state emission from TiO_2 nanoparticles in microemulsion solutions // *Langmuir*, **17**, p. 4129-4130 (2001).
49. B. Ohler and W. Langel, Molecular dynamics simulations on the interface between titanium dioxide and water droplets: A new model for the contact angle // *J. Phys. Chem. C*, **113**, No.23, p. 10189-10197 (2009).
40. F. Allegretti, S. O'Brien, M. Polcik, D.I. Sayago, and D.P. Woodruff, Adsorption bond length for H_2O on TiO_2(110): A key parameter for theoretical understanding // *Phys. Rev. Lett.* **95**, p. 226104 (2005).
41. R. Luschtinetz, J. Frenzel, T. Milek, G. Seifert, Adsorption of phosphonic acid at the TiO_2 anatase (101) and rutile (110) surfaces // *J. Phys. Chem. C*, **113**, No.14, p. 5730-5740 (2009).
42. D. Wu, J. Liu, X. Zhao, A. Li, Y. Chen, N. Ming, Sequence of events for the formation of titanate nanotubes, nanofibers, nanowires, and nanobelts // *Chem. Mater*., **18**, No.2, p. 547-553 (2006).
43. B. Zhu, Z. Sui, S. Wang, X. Chen, S. Zhang, S. Wu, W. Huang, Alternative approaches to fabrication of gold-modified TiO_2 nanotubes // *Materials research bulletin* **41**, p. 1097-1104 (2006).
44. S. Zhang, L.-M. Peng, Q. Chen, G.H. Du, G. Dawson, and W.Z. Zhou, Formation mechanism of $H_2Ti_3O_7$ nanotubes // *Phys. Rev. Lett.* **91**, No.25, p. 256103 (2003).
45. R. Menzel, A.M. Peiro, J.R. Durrant, M.S.P. Shaffer, Impact of hydrothermal processing conditions on high aspect ratio titanate nano-structures // *Chem Mater*., **18**, p. 6059-6068 (2006).
46. B.D. Yao, Y.F. Chan, X.Y. Zhang, W.F. Zhang, Z.Y. Yang, N. Wang, Formation mechanism of TiO_2 nanotubes // *Appl. Phys. Lett*., **82**, No.2, p. 281-283 (2003).
47. J.S. Jang, S.H. Choi, D.H. Kim, J.W. Jang, K.S. Lee, J.S. Lee, Enhanced photocatalytic hydrogen production from water-methanol solution by nickel intercalated into titanate nanotube // *J. Phys. Chem. C*, **113**, No.20, p. 8990-8996 (2009).
48. S. Zhang, Q. Chen, L.-M. Peng, Structure and formation of $H_2Ti_3O_7$ nanotubes in an alkali environment // *Phys. Rev. B*, **71**, p. 014104 (2005).
49. D. Wang, F. Zhou, Y. Liu, W. Liu, Synthesis and characterization of anatase TiO_2 nanotubes with uniform diameter from titanium powder // *Mater. Lett.* **62**, p. 1819-1822 (2008).
50. J.P. Xu, S.B. Shi, L. Li, J.F. Wang, L.Y. Lv, F.M. Zhang, Y.W. Du, Effect of manganese ions concentration on the anatase-rutile phase transformation of TiO_2 films // *J. Phys. Chem. Solids* **70**, p. 511-515 (2009).
51. Y.V. Kolen'ko, K.A. Kovnir, A.I. Gavrilov, A.V. Garshev, P.E. Meskin, B.R. Churagulov, M. Bouchard, C. Colbeau-Justin, O.I. Lebedev, G. Van Tendeloo, M. Yoshimura, Structural, textural, and electronic properties of a nanosized mesoporous $Zn_xTi_{1-x}O_{2-x}$ solid solution prepared by a supercritical drying route // *J. Phys. Chem. B*, **109**, No.43, p. 20303-20309 (2005).